Biogeosciences Discuss., 8, 6265–6280, 2011
www.biogeosciences-discuss.net/8/6265/2011/
doi:10.5194/bgd-8-6265-2011

Biogeosciences Discussions

The combined impact of CO_2-dependent parameterisations of Redfield and Rain ratios on ocean carbonate saturation

K. F. Kvale[1], K. J. Meissner[1], M. d'Orgeville[1], R. J. Matear[2], B. I. McNeil[1], and M. H. England[1]

[1]Climate Change Research Centre, University of New South Wales, Sydney, NSW, Australia
[2]CSIRO, Hobart, TAS, Australia

Received: 14 June 2011 – Accepted: 20 June 201 – Published: 30 June 2011

Correspondence to: K. F. Kvale (k.kvale@unsw.edu.au)

Published by Copernicus Publications on behalf of the European Geosciences Union.

Abstract

Future changes to the organic carbon and carbonate pumps are likely to affect ocean ecosystem dynamics and the biogeochemical climate. Here, biological dependencies on the Rain and Redfield ratios on pCO_2 are implemented in a coupled Biogeochemistry-Ocean Model, the CSIRO-Mk3L, to establish extreme-case carbonate saturation vulnerability to model parameterisation at year 2500 using IPCC Representative Concentration Pathway 8.5. Surface carbonate saturation is relatively insensitive to the combined effects of variable Rain and Redfield ratios (an anomaly of less than 10 % of the corresponding change in the control configuration by year 2500), but the global zonally-averaged ocean interior anomaly due to these feedbacks is up to 130 % by 2500. A non-linear interaction between organic and carbonate pumps is found in export production, where higher rates of photosynthesis enhance calcification by raising surface alkalinity. This non-linear effect has a negligible influence on surface carbonate saturation but does significantly influence ocean interior carbonate saturation fields (an anomaly of up to 45 % in 2500). The strongest linear and non-linear sensitivity to combined feedbacks occurs in low-latitude remineralisation zones below regions of enhanced biological production, where dissolved inorganic carbon rapidly accumulates.

1 Introduction

The marine organic carbon and carbonate pumps are affected by increasing atmospheric carbon dioxide (CO_2) concentrations through marine organisms. Enhanced CO_2 in seawater has been observed to increase the rate of particulate organic carbon (POC) production by enhancing photosynthesis (Eq. 1), termed the "POC production feedback" (Zondervan et al., 2001).

$$106\ CO_2 + 16\ NO_3^- + HPO_4^{2-} + 78\ H_2O + 18\ H^+ \longrightarrow C_{106}H_{175}O_{42}N_{16}P + 150\ O_2. \quad (1)$$

Mesocosm experiments by Riebesell et al. (2007) suggest the above fixed carbon-to-phosphate stoichiometry (the Redfield ratio) may vary by as much as a factor of 6 under high-pCO_2 conditions, significantly altering the efficiency of primary producers consuming DIC and reducing the effect of nutrient limitation. There are important biogeochemical impacts from enhanced POC production efficiency related to remineralisation, e.g. expanding suboxic zones (Oschlies et al., 2008) and adjustments in carbonate compensation horizon and pH (Boudreau et al., 2010).

The availability of carbonate for biological calcification (Eq. 2) is measured as calcium carbonate saturation (Ω), where the concentrations of calcium and calcite are divided by a solubility constant K_{sp} (Eq. 3).

$$Ca^{2+} + 2HCO_3^- \longrightarrow CaCO_3 + CO_{2(aq)} + H_2O \quad (2)$$

$$\Omega = \frac{\left[Ca^{2+}\right]\left[CO_3^{2-}\right]}{K_{sp}} \quad (3)$$

The reduction of biological carbonate production (particulate inorganic carbon, PIC) as a response to increased pCO_2 means less CO_2 is released to the surface mixed layer as a by-product of calcification. The most salient effects of this "CO_2-calcification feedback" are resulting changes to nutrient and carbonate profiles which could impact on ecosystem dynamics (e.g., Ridgwell et al., 2007; Boudreau et al., 2010). As atmospheric CO_2 increases, the combined effect of reduced PIC production and export in addition to accelerated POC production presents the possibility of truncated nutrient and carbon recycling, reorganising ocean basin nutrient and carbon profiles over the long term. Of particular interest are the low latitudes which have been shown to be disproportionately vulnerable to the biogeochemical effects of enhanced POC production in the studies mentioned above. The net effect of combined organic and inorganic carbon production and export feedbacks on inorganic carbonate chemistry is addressed from a global mean perspective in a recent study by Boudreau et al. (2010), who used a four box model and found a deep ocean response in global interior pH,

carbonate compensation depth and snowline depth which increased from minimal over a century time-scale to a substantial impact over the duration of their millennial runs. They also demonstrate latitudinal variation in the solubility pump owing to production feedbacks, with increasing organic production in low latitude surface waters (Boudreau et al., 2010).

While the Boudreau et al. (2010) box model is able to capture biogeochemical differences between high and low latitude surface (to 100 m depth) and the global deep ocean response to CO_2 forcing, nutrient pooling as a result of changes to remineralisation have been shown to concentrate between 200–800 m (Hofmann and Schellnhuber, 2009). In this study, the relative importance of combined organic and carbonate production feedbacks in governing regional carbonate chemistry in an ocean general circulation model is examined for a future climate scenario with high CO_2 emissions.

2 Model and experimental design

The coupled climate-carbon model, CSIRO-Mk3L (Phipps, 2010), is employed in ocean-only mode, as the focus of the study is ocean biogeochemistry. The Mk3L ocean has a resolution of 2.8° longitude by 1.6° latitude with 21 vertical levels, with a similar structure to the higher-resolution CSIRO Mk3 and CSIRO Mk2 models (Gordon et al., 2002; Hirst et al., 1996). The background mean ocean circulation simulation has been described previously by Najjar et al. (2007); Dutay et al. (2002). The ocean biogeochemistry component of Mk3L follows Matear and Hirst (2003), using OCMIP protocol (Dutay et al., 2002) for CO_2 air/sea gas exchange and carbonate chemistry.

In order to explore the interaction between biological carbon pump feedbacks, dependencies on pCO_2 are added to the fixed Redfield carbon-to-phosphate (POC : POP) and carbonate-to-phosphate (PIC : POP, the Rain ratio) parameterisations. POC export (F^{POC}) and POP export (F^{POP}) are varied with a linear response scaled against

pre-industrial ocean pCO_2 (Riebesell et al., 2007):

$$F^{POC} = 106\, F^{POP} F_{scale} \quad (4)$$

$$F_{scale} = 1 + \frac{2}{700}\frac{16}{106}(pCO_2 - 280). \quad (5)$$

Remineralisation of POC follows this same scaling, so not only is a greater proportion of POC exported from the surface with respect to POP, a greater proportion is also remineralised.

Biological calcification in the model contains an additional scaling factor from Ridgwell et al. (2007) to vary carbonate production (γ) with local calcite saturation, where η is a power parameter (with a value of 0.81) controlling the non-linearity of the calcification response.

$$\gamma = (\Omega - 1)^{\eta} \quad \text{For } \Omega > 1.0 \quad (6)$$

$$\gamma = 0.0 \quad \text{For } \Omega \leq 1.0 \quad (7)$$

Carbonate export (F^{PIC}) is linked to POP export by a calculated Rain ratio modified by γ:

$$F^{PIC} = \gamma \times r_0^{PIC:POC} \times F^{POP} \times r_0^{POC:POP} \quad (8)$$

where $r_0^{PIC:POC}$ is a globally fixed ratio (Ridgwell et al., 2007) and $r_0^{POC:POP}$ is fixed following Eq. (4) without the Redfield scaling factor F_{scale}. Note that carbonate export is used as a proxy for calcite production- other parameterisations exist; Ridgwell et al. (2009) and Gangsto et al. (2010) provide two recent reviews. The Ridgwell et al. (2007) parameterisation is one of the more sensitive parameterisations (Ridgwell et al., 2009), and is therefore applied to this study for examining high-end vulnerability. This Rain ratio parameterisation does not account for particle aggregation, nor does it differentiate between particle classes, but it does demonstrate a latitudinal dependency which roughly aligns with observations, owing to the calcite saturation scaling factor γ.

Following OCMIP protocol (Dutay et al., 2002), model PIC dissolution below the surface layer utilises a rigid exponential depth dependency so changes to surface PIC production mostly affect the depth of complete PIC dissolution; i.e. increasing PIC production yields a more penetrating PIC inorganic chemical signal in the water column. The current arrangement maintains independence between inorganic and organic carbon pump feedbacks while allowing for interactions with carbonate chemistry from both. Note this independence is only true below the surface; the scaling factors applied at the surface for PIC and POC with respect to POP (Eqs. 4 and 8) allow for direct interaction between organic and inorganic export feedbacks via alteration of surface pCO_2 and calcite saturation.

Four different configurations of the model (CONTROL, RAIN, REDFIELD, RAINRED) are spun up for six thousand years under a constant atmospheric concentration of 278 ppm to reach pre-industrial equilibrium, and are then forced by an atmospheric carbon concentration pathway following RCP8.5 (Riahi et al., 2007) to 2500. This scenario exhibits growth in atmospheric CO_2 concentrations to 936 ppm by 2100 and 1962 ppm by 2250, whereupon the concentration remains constant until 2500. The CONTROL configuration utilises globally uniform fixed Redfield (Eq. 1) and Rain ratios (PIC : POP value of 8.48). The RAIN configuration parameterises the Rain ratio following Ridgwell et al. (2007, Eqs. 2 to 3 and 6 to 8), where $r_0^{PIC:POC}$ is set to 0.02 (the negative one standard deviate given in Ridgwell et al., 2007) and the Rain ratio is solved prognostically. The REDFIELD configuration fixes the Rain ratio using the CONTROL value but varies Redfield stoichiometry according to Eqs. (4) and (5). Finally, RAINRED varies both Rain and Redfield ratios. Note only PIC and POC vary between runs; POP does not change across configurations. Also, as this is an ocean-only model, increasing CO_2 concentrations in the experiments impact neither the global radiative balance nor ocean circulation, and no physical feedback to atmospheric CO_2 is simulated.

3 Transient simulations

3.1 PIC and POC surface export

Rain and Redfield feedbacks alter PIC and POC export from the surface layer. Figure 1 summarises globally integrated annual surface carbon export from year 1900 to year 2500 for each configuration. PIC and POC export remain constant over the CONTROL simulation (red lines) because both Rain and Redfield feedbacks are fixed constants. RAIN (blue stars) PIC export decreases relative to CONTROL because as surface calcite saturation decreases with increasing pCO_2, less calcification occurs in the surface layer and less PIC is exported. RAIN PIC also has a lower inital value from CONTROL owing to this export dependence on surface calcite saturation. POC export is unaffected by changes to the Rain ratio and hence RAIN POC mirrors CONTROL POC. PIC export in the REDFIELD experiment (green diamonds) is unaffected by changes in Redfield stoichiometry and hence REDFIELD PIC mirrors CONTROL PIC. The POC field in RAINRED (black lines) mirrors that of REDFIELD POC, which like REDFIELD sees increases in POC export as pCO_2 increases the efficiency of the organic carbon pump. Initial POC values for REDFIELD and RAINRED are slightly higher than those of RAIN and CONTROL owing to the dependence of export on pCO_2 anomaly from 278 ppm, which has increased by year 1900. Note that RAINRED PIC does not exactly mirror RAIN PIC, even though in the REDFIELD configuration PIC export is shown to be unaffected. This incongruence reveals a "non-linear" exchange between Rain and Redfield feedbacks in the combined RAINRED simulation, where reduced PIC export (calcification) due to the decreasing carbonate saturation in the inorganic carbon pump is slightly tempered by the additional release of carbonate owing to an enhanced organic carbon pump. This chemical exchange is summarised in Fig. 2 and revolves about the enhanced consumption of free hydrogen in Eq. (1) as part of enhanced POC formation. Inorganic carbon chemistry dictates a reduction in free hydrogen resulting in an addition of carbonate ions, according to $HCO_3^- \rightleftharpoons H^+ + CO_3^{2-}$. This small increase in carbonate ion buffers the carbonate saturation which controls PIC export production

in the model (shown as a blue pathway). In the RAINRED configuration, PIC formation is still reduced by the decreased saturation (yellow pathway), but not as much as it is in the RAIN configuration where no additional carbonate input from altered photosynthesis occurs.

3.2 Carbonate saturation

The impact of variable PIC and POC export production on ocean carbonate saturation in the RAINRED configuration can be quantified using snapshot and anomaly plots, shown in Fig. 3. Pre-industrial calcite saturation is shown as a global zonal mean (top left panel), and map cross-sections at 1000 m (top middle panel) and 3000 m (top right panel). RAINRED calcite saturation at year 2500 is shown for the same spatial configuration in the second row. By 2500 only a shallow region between 40° North and South latitude meets the PIC production criteria (Eq. 6). In the third row, RCP8.5 forcing over the simulation is removed by subtracting the pre-industrial equilibrium state from 2500, and then subtracting that difference for the CONTROL run from the remainder (e.g., ΔRAINRED – ΔCONTROL where Δ is year of simulation minus pre-industrial state). The non-linear component of these anomalies are shown in the bottom row. Positive non-linear anomaly values indicate a mitigation response for carbonate saturation. Negative non-linear anomaly values indicate an amplification of the carbonate saturation anomaly.

A striking pattern emerges in the additional total and non-linear effects of the combined feedbacks (Fig. 3). By 2500 the global zonally averaged RAINRED anomaly is up to 0.25 units larger than that of CONTROL in the tropical abyssal ocean (third row, leftmost panel), an anomaly more than twice as large as the change in ΔCONTROL over this time (not shown). The RAINRED anomaly contributes up to 45 % of the global zonally averaged background RAINRED carbonate saturation in this same region, even though the additional impact on carbonate saturation at the surface is less than 10 % (seen when comparing leftmost panels in the second and third rows). This increasing impact on carbonate saturation in the ocean interior away from the surface is due to the

decoupling of PIC and POC remineralisation owing to differing remineralisation length scales, where POC remineralisation is accelerated by the variable Redfield ratio but PIC dissolution varies in depth of complete dissolution only.

A positive (mitigative) non-linear response is present in the ocean interior (bottom left panel), and is valued at roughly 10 % of the global zonally averaged RAINRED anomaly (seen when comparing leftmost panels in the third and fourth rows). A weak negative non-linear response is found in the upper 500 m (up to 1.5 % of ΔCONTROL, not shown). This non-linear RAINRED amplification at the surface and mitigation at depth is due to the non-linear effect of POC enhancement on PIC production described earlier and shown in Fig. 2. Reduction of PIC export production in RAINRED is tempered by the additional availability of carbonate owing to enhanced POC production, which allows for slightly reduced carbonate saturation at the surface and enhanced saturation at depth, relative to what would be seen in purely independent carbon and inorganic carbon pump feedbacks.

Tropical regions show greater variability in Ω than what the global mean profile plots suggest. Figure 3 middle and right columns show the strongest impacts on carbonate saturation are confined to regions with strong POC enhancement, such as upwelling zones in eastern ocean basins. Linear and non-linear RAINRED anomalies in these regions are the largest below depths of complete PIC dissolution, hence are more apparent in the 3000 m depth plots (right column) than the 1000 m plots (middle column). The Eastern Pacific in particular shows the strongest response, where the ΔRAINRED anomaly is over 0.3 units at 3000 m depth (third row, right panel), a saturation change eight times that of ΔCONTROL in this same region (not shown). The non-linear anomaly (bottom right panel) in this region is also significant, with a mitigating effect of about 20 % the RAINRED anomaly value in this region (seen when comparing rightmost panels in the third and fourth row). As POC production is most enhanced in this region, the impact on PIC export production extends the deepest within this region by the fixed PIC dissolution gradient. In contrast to the eastern Pacific, the Indian Ocean has generally less POC and PIC production and hence has

a weaker non-linear signal. While enhanced carbonate undersaturation and a small non-linear positive anomaly are seen by year 2500 in the Indian Ocean, the signal does not extend as deep as in the Pacific and the maximum non-linear anomaly values peak around 1000 m depth (bottom middle panel).

4 Summary and conclusions

This study has demonstrated the sensitivity of the interior ocean carbonate saturation to the combined effects of varying Redfield and Rain ratios. This builds upon previous work, most notably Boudreau et al. (2010), who calculated a strong combined Rain and Redfield feedback on ocean interior pH and carbonate compensation depth in a box model. These results show that biogeochemical feedbacks have the potential to significantly alter carbonate saturation without coincident changes in the mean circulation, and may explain at least part of a mechanism operating around high carbon perturbation events in the past, when calcification shows evidence of both lasting and preferential depression with respect to other forms of production (as reviewed by Veron, 2008), even in the absence of a stagnant circulation (e.g., Winguth and Maier-Reimer, 2005). It must, however, be stressed that this study is a sensitivity study of biogeochemical parameterisations. Results are not projections of future ocean chemical climate because the model includes neither sediments nor radiative feedback. Likewise, the parameterisations reflect observed responses of an incomplete sampling of the biodiversity found in the global ocean, with the REDFIELD parameterisation in particular tested beyond its calibration limit of 1050 ppm. Additional experimental limitations might include nutrient trapping as a side-effect of model resolution (e.g., Aumont et al., 1999), which would contribute to an overestimate of the magnitude of the combined effect, though this is likely a small influence as only anomalies are discussed and circulation remains unchanged in the experiments. The insensitivity of PIC export to Ω might, on the other hand, be contributing to an underestimate of the combined effect by artificially lowering the depth of PIC dissolution below the zone of POC remineralisation. While

the physical justification of widespread Ω-dependent PIC export is debatable (as summarised by Sarmiento and Gruber, 2006, pages 371–374), severely undersaturated water such as what is calculated in this hypothetical parameter test does approach a calcite dissolution e-folding timescale of a similar order to that of carbonate particle sinking. Should subsurface pooling of DIC owing to enhanced POC export and remineralisation accelerate PIC dissolution, the non-linear carbonate anomaly would be enhanced following the deep ocean schematic in Fig. 2.

CO_2 calcification and POC production feedbacks operate in the same region of the ocean interior and may both mitigate and enhance each other. As such, caution is warranted when assessing ocean carbonate chemistry using only one feedback at a time. This is particularly true in the low-latitude sub-surface and abyssal ocean regions, which show particular sensitivity to the non-linear contribution of the dual feedbacks of varying Redfield and Rain ratios. As carbonate saturation is a commonly accepted proxy for calcification, such a sensitivity has relevance for predicting changes in ecosystem dynamics in an increasingly acidic marine environment.

Acknowledgements. KM, BM, ME and MD are supported by the Australian Research Council.

References

Aumont, O., Orr, J., Monfray, P., Madec, G., and Maier-Reimer, E.: Nutrient trapping in the equatorial Pacific: the ocean circulation solution, Global Biogeochem. Cy., 13, 351–369, 1999. 6274

Boudreau, B. P., Middelburg, J. J., Hofmann, A. F., and Meysman, F. J. R.: Ongoing transients in carbonate compensation, Global Biogeochem. Cy., 24, GB4010, 13 pp., doi:10.1029/2009GB003654, 2010. 6267, 6268, 6274

Dutay, J.-C., Bullister, J., Doney, S., Orr, J., Najjar, R., Caldeira, K., Campin, J.-M., Drange, H., Follows, M., Gao, Y., Gruber, N., Hecht, M., Ishida, A., Joos, F., Lindsay, K., Madec, G., Maier-Reimer, E., Marshall, J., Matear, R., Monfray, P., Mouchet, A., Plattner, J., Sarmiento, J., Schlitzer, R., Slater, R., Totterdell, I., Weirig, M.-F., Yamanaka, Y., and Yool, A.: Evaluation

of ocean model ventilation with CFC-11: comparison of 13 global ocean models, Ocean Model., 4, 89–120, 2002. 6268, 6270

Gangstø, R., Joos, F., and Gehlen, M.: Sensitivity of pelagic calcification to ocean acidification, Biogeosciences, 8, 433–458, doi:10.5194/bg-8-433-2011, 2011. 6269

Gordon, H., Rotstayn, L., McGregor, J., Dix, M., Kowalczyk, E., O'Farrell, S., Waterman, L., Hirst, A., Wilson, S., Collier, M., Watterson, I., and Elliott, T.: The CSIRO Mk3 Climate System Model, Technical Paper 60, CSIRO Atmospheric Research, 2002. 6268

Hirst, A., Gordon, H., and O'Farrell, S.: Global warming in a coupled climate model including oceanic eddy-induced advection, Geophys. Res. Lett., 23, 3361–3364, 1996. 6268

Hofmann, M. and Schellnhuber, H.-J.: Oceanic acidification affects marine carbon pump and triggers extended marine oxygen holes, P. Natl. Acad. Sci. USA, 106, 3017–3022, doi:10.1073/pnas.0813384106, 2009. 6268

Matear, R. and Hirst, A.: Long-term changes in dissolved oxygen concentrations in the ocean caused by protracted global warming, Global Biogeochem. Cy., 17, 1125 pp., doi:10.1029/2002GB001997, 2003. 6268

Najjar, R. G., Jin, X., Louanchi, F., Aumont, O., Caldeira, K., Doney, S. C., Dutay, J.-C., Follows, M., Gruber, N., Joos, F., Lindsay, K., Maier-Reimer, E., Matear, R. J., Matsumoto, K., Monfray, P., Mouchet, A., Orr, J. C., Plattner, G.-K., Sarmiento, J. L., Schlitzer, R., Slater, R. D., Weirig, M.-F., Yamanaka, Y., and Yool, A.: Impact of circulation on export production, dissolved organic matter, and dissolved oxygen in the ocean: results from phase II of the ocean carbon-cycle model intercomparison project (OCMIP-2), Global Biogeochem. Cy., 21, GB3007, doi:10.1029/2006GB002857, 2007. 6268

Oschlies, A., Schulz, K. G., Riebesell, U., and Schmittner, A.: Simulated 21st century's increase in oceanic suboxia by CO_2-enhanced biotic carbon export, Global Biogeochem. Cy., 22, GB4008, doi:10.1029/2007GB003147, 2008. 6267

Phipps, S.: The CSIRO Mk3L climate system model v1.2, Technical report, Antarctic Climate and Ecosystems Cooperative Research Centre, 2010. 6268

Riahi, K., Gruebler, A., and Nakicenovic, N.: Scenarios of long-term socio-economic and environmental development under climate stabilization, Technol. Forecast. Soc., 74, 887–935, 2007. 6270

Ridgwell, A., Zondervan, I., Hargreaves, J. C., Bijma, J., and Lenton, T. M.: Assessing the potential long-term increase of oceanic fossil fuel CO_2 uptake due to CO_2-calcification feedback, Biogeosciences, 4, 481–492, doi:10.5194/bg-4-481-2007, 2007. 6267, 6269, 6270

Ridgwell, A., Schmidt, D. N., Turley, C., Brownlee, C., Maldonado, M. T., Tortell, P., and Young, J. R.: From laboratory manipulations to Earth system models: scaling calcification impacts of ocean acidification, Biogeosciences, 6, 2611–2623, doi:10.5194/bg-6-2611-2009, 2009. 6269

Riebesell, U., Schulz, K. G., Bellerby, R. G. J., Botros, M.and Fritsche, P., Meyerhoefer, M., Neill, C., Nondal, G., Oschlies, A., Wohlers, J., and Zoellner, E.: Enhanced biological carbon consumption in a high CO_2 ocean, Nature, 450, 545–548, doi:10.1038/nature06267, 2007. 6267, 6269

Sarmiento, J. and Gruber, N.: Ocean Biogeochemical Dynamics, Princeton University Press, Princeton and Oxford, 2006. 6275

Veron, J. E. N.: Mass extinctions and ocean acidification: biological constraints on geological dilemmas, Coral Reefs, 27, 459–472, doi:10.1007/s00338-008-0381-8, 2008. 6274

Winguth, A. and Maier-Reimer, E.: Causes of the marine productivity and oxygen changes associated with the Permian-Triassic boundary: A reevaluation with ocean general circulation models, Mar. Geol., 217, 283–304, doi:10.1016/j.margeo.2005.02.011, 2005. 6274

Zondervan, I., Zeebe, R., Rost, B., and Riebesell, U.: Decreasing marine biogenic calcification: a negative feedback on rising atmospheric pCO_2, Global Biogeochem. Cy., 15, 507–516, 2001. 6266

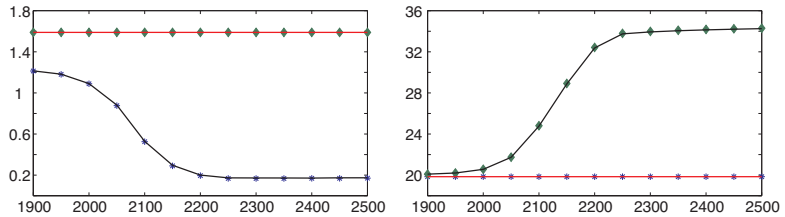

Fig. 1. Timeseries of integrated global PIC (left plot) and POC (right plot) surface export production in Pg C per year. Color key is as follows: CONTROL (red), RAIN (blue), REDFIELD (green), RAINRED (black).

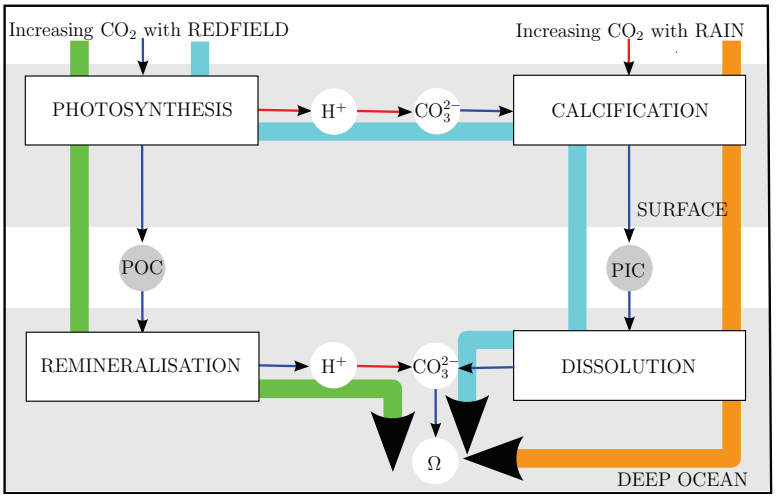

Fig. 2. Schematic of feedback processes operating between organic and inorganic carbon pumps and carbonate saturation. Positive feedbacks are presented in thin blue and negative feedbacks in thin red. An even number of negative feedbacks (red arrows) sum to a positive feedback, while an odd number of negative feedbacks remain negative. The impact of the variable Rain and Redfield ratio parameterisations on deep ocean carbonate saturation are shown as fat arrows: Rain (yellow), Redfield (green), Rain and Redfield (blue).

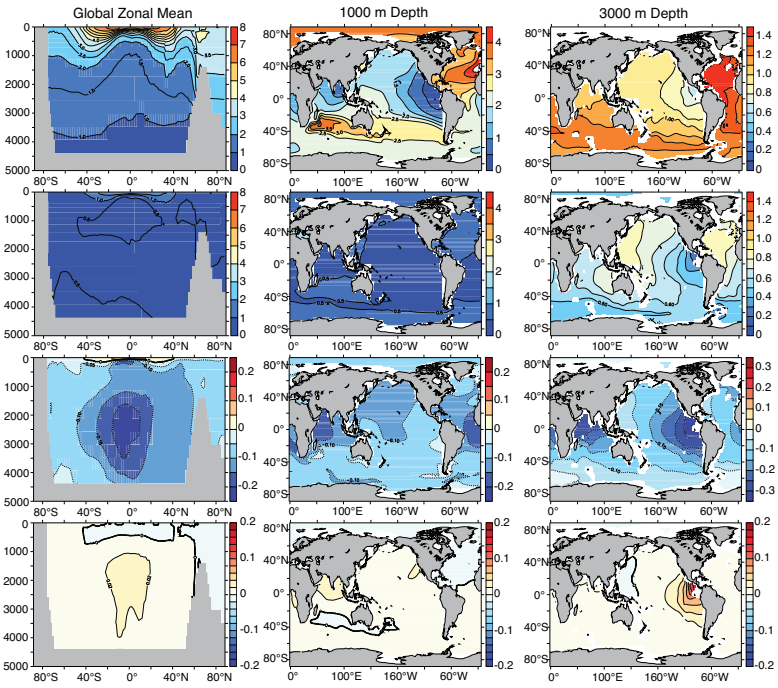

Fig. 3. Pre-industrial (first row) and year 2500 (second row) RAINRED calcite saturation, and year 2500 RAINRED calcite saturation linear (ΔRAINRED – ΔCONTROL, third row) and non-linear (ΔRAINRED – (ΔRAIN + ΔREDFIELD), fourth row) anomalies. Left column shows the global zonal mean. Middle column is a map view at 1000 m depth. Right column is a map view at 3000 m depth.